THE JOURNAL OF PHYSICAL CHEMISTRY C

Article

Cite This: J. Phys. Chem. C 2019, 123, 24807−24817

pubs.acs.org/JPCC

Interplay between Conjugated Backbone Units and Side Alkyl Groups in Chirality Sensitive Interactions of Single Walled Carbon Nanotubes with Polyfluorenes

Brendan J. Gifford,[†,‡,§] Braden M. Weight,[‡,§,#] and Svetlana Kilina*[,§]

[†]Center for Nonlinear Studies, [‡]Center for Integrated Nanotechnologies, Los Alamos National Laboratory, Los Alamos, New Mexico 87545, United States

[§]Chemistry and Biochemistry Department, North Dakota State University, Fargo, North Dakota 58102, United States

[#]Physics Department, North Dakota State University, Fargo, North Dakota 58102, United States

Supporting Information

ABSTRACT: Current synthetic methods of single walled carbon nanotubes (SWCNTs) fail to produce monodisperse chiralities resulting in the need for postsynthetic separation relying on selectively dispersed SWCNTs with conjugated polymers such as poly(9,9-di-*n*-octylfluorenyl-2,7-diyl) (PFO) and its derivatives. However, the mechanism of PFO binding to SWCNTs of certain chiralities is not well understood. Using force field calculations we show that $\pi-\pi$ stacking between the SWCNT and PFO backbone units provides the predominant force holding the polymer−SWCNT complex together, while interactions with the side alkyl chains are critical for the chirality selectivity. Short side chains introduce additional van der Waals interactions stabilizing the PFO-SWCNT system independent of the chirality, while long side chains with eight and more carbons distort the PFO geometry reducing $\pi-\pi$ interactions and increasing the wrapping angle of the PFO about the SWCNT being sensitive to chiralities. The optimal strength of interaction is achieved for octyl groups due to increased van der Waals interactions compensating decrease in $\pi-\pi$ stacking. In contrast to expectations, our simulations reveal that a perfect $\pi-\pi$ stacking between the SWCNT and PFO does not differentiate between different tube chiralities and is not responsible for their selectivity.

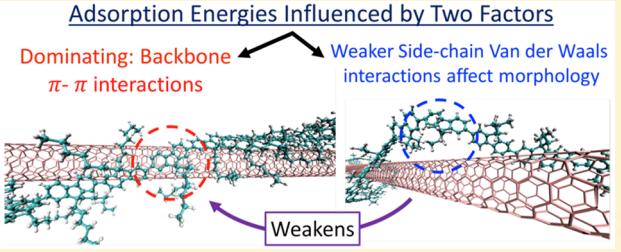

INTRODUCTION

Single walled carbon nanotubes (SWCNTs) are pseudo one-dimensional nanostructures composed of hexagonal rings of sp^2 hybridized carbon atoms.[1,2] Their electronic and optical properties depend on their geometry—in particular, their chiralities and diameters—resulting in metallic or semiconducting structures with optical gaps varying from the IR to visible energy range.[3,4] Strong absorption is typically observed for excitations from 400 to 1600 nm,[5] making SWCNTs useful for integration into the active layers of photovoltaic devices.[6−8] Their optical transparency and the ability to tune electronic levels via modifications to their geometry lends promise to their application as hole-injection layers in light emitting diodes.[9,10] SWCNTs have been also proposed as active layers in chemical and biological sensors, benefiting from their high surface to volume ratio and superior electron transport properties.[11−16]

However, to move from the proof-of-concept stage to implementation in devices, uniform SWCNTs samples containing nanotubes of the same diameter and chirality are required. This desire, especially for chirality specific SWCNT samples, has been a significant challenge for synthetic efforts for the past two decades. While recent advances have enabled the production of monodisperse samples,[17] synthesis of a single chirality of SWCNT has thus far eluded experimental efforts. To resolve this challenge, a number of different isolation methods have been utilized to postsynthetically isolate SWCNTs of a desired chirality. This involves the utilization a variety of techniques including density differentiation by centrifugation,[18,19] size exclusion chromatography,[20−22] electrophoresis,[23] and combinations of these methods. Additionally, various surfactants are used to disperse and dissolve SWCNTs and selectively interact with tubes of a specific chirality and electronic type.[24] Deoxyribonucleic acid (DNA) is among the surfactants that have shown the ability to selectively interact with SWCNT of specific chiralities, as was predicted theoretically[25,26] and realized experimentally.[27−29]

Another class of surfactants that receives significant attention for the purpose of separation of chirality specific SWCNTs is conjugated polymers, which benefit from a lower synthetic cost. Many experimental studies have defined specific conjugated polymer systems that can be used for SWCNT chirality separation.[30−36] In particular, poly(9,9-di-*n*-octylfluorenyl-2,7-

Received: May 22, 2019
Revised: August 8, 2019
Published: August 29, 2019

DOI: 10.1021/acs.jpcc.9b04869
J. Phys. Chem. C 2019, 123, 24807−24817

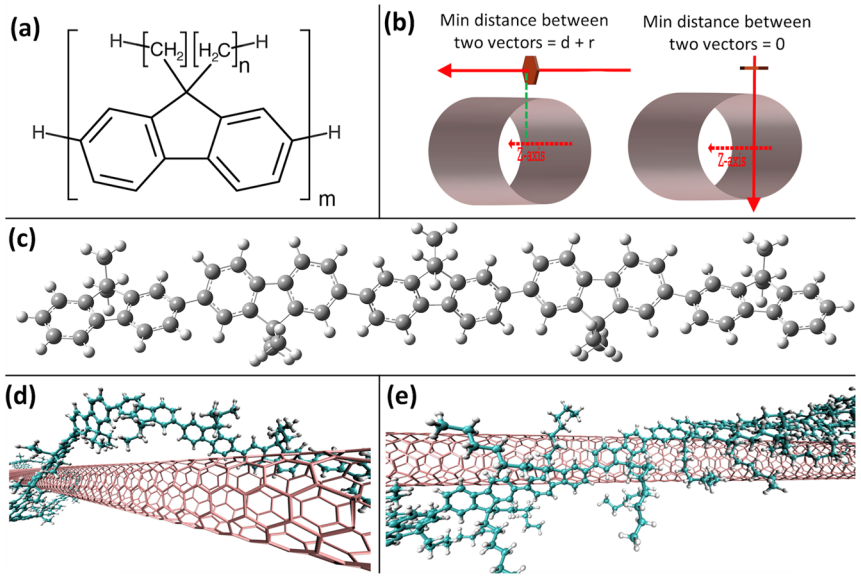

Figure 1. Structures of PFO and (6,5) SWCNT functionalized by PFO. (a) Schematic representation of a single unit (a monomer) of PFO where *n* is the number of methylene groups in the alkyl side chain and *m* is the degree of polymerization. (b) Limits of the twisting parameter defining the alignment between the PFO backbone unit and the SWCNT surface. A value of zero indicates that the normal vector to the polymer unit intersects with the axis of the SWCNT, thereby maximizing $\pi-\pi$ stacking. A value of one indicates that the polymer unit is perpendicular to the surface of the SWCNT, and therefore the minimum distance between the vector normal to the unit and the SWCNT axis is equal to the radius of the SWCNT, r, plus the distance between the SWCNT and the center of mass of the polymer unit, d. (c) PFO pentamer (m = 5) optimized with DFT using the B3LYP functional and the 6-31G* basis set from which the MM3 force field was reparameterized. (d) and (e) The MM3-optimized geometries of the SWCNT and 40-mer PFO with methylethyl (n = 3) and octyl (n = 8) groups, respectively.

diyl) (PFO)[33,37] and its derivatives[32,38] have shown an exceptional ability in selective dispersion and enrichment of specific SWCNT chiralities, especially for tubes of small diameter and large chiral angles.[39] However, these discoveries are empirical, and properties governing the effectiveness of selective sorting of SWNTs based on the chemical structures of polymers are not yet well understood yet. A detailed understanding of the interactions between PFO and SWCNTs is essential for use of efficient sorting of specific SWCNT chiralities for use in specific applications.

A number of computations have complemented experimental studies with the goal of establishing a relationship between the electronic and morphological properties of such polymer-SWCNT systems,[30,36,40−47] and thus assist in rational design of the best polymer candidates for SWCNT functionalization. For computations, it is optimal that all interactions be taken into account. Conjugated materials such as SWCNTs and conducting polymers possess attractive, noncovalent interactions between aromatic rings with sp^2-hybredized bonds, referred to as "$\pi-\pi$ interaction" or "$\pi-\pi$ stacking". The resulting morphology of the conjugated polymer on the surface of the SWCNT is dictated by such $\pi-\pi$ interactions, the stabilization of which originates from a balance between quadrupole/quadrupole and London dispersion forces.[48] Due to their less polarizable nature, sp^3-hybridized orbitals of alkyl side chains interact with the sp^2-hybridized orbitals of the SWCNT to a weaker degree. Herein, this interaction between sp^3-hybridized carbons of alkyl side chains with the sp^2-hybredized carbons of the SWCNT is referred to as "van der Waals" interaction.

A common assumption in computational studies involving SWCNT-polymer systems is that the predominant interactions between the conjugated polymer and SWCNT involve $\pi-\pi$ stacking.[40,45] As such, the large alkyl groups, which are typically present in the polymer and provide their remarkable solubility and dispersion abilities, are frequently omitted in computational studies. While such an approximation allows for the simplification of the models and reduction of the computational cost, it also results in the complete neglect of van der Waals interactions between side alkyl groups and the SWCNT. Despite their weak nature, these interactions still contribute to the adsorption energy of the conjugated polymer to SWCNTs and, therefore, may play a nontrivial role in both dispersion and selectivity abilities of such conjugated polymers, as was eluded in experiments.[32,33,49] Determination of the degree to which change of the side chain length affects the polymer binding to the SWCNT is a goal of the current study.

Here we systematically determine the effect of alkyl side groups of PFO oligomers on the morphology and adsorption energy to various SWCNTs, as illustrated in Figure 1. This is accomplished through molecular dynamics (MD) simulations using reparameterized MM3 force field. Instead of generating long trajectories of molecular dynamics simulations, we have reduced computational expense by optimizing a diverse set of starting geometries with various initial wrapping angles of the PFO around the SWCNT to introduce stochasticity. In contrast to previous studies focusing on only a few SWCNTs of diameters larger than 1.2 nm interacting with PFO with long alkyl chains,[32] the current study considers a dozen different chiralities of narrow nanotubes with the diameter range from 0.6 to 1.1 nm, which typically coexist in SWCNT samples prepared by CoMoCat[50] and HiPCO[51] methods. These SWCNTs are noncovalently functionalized by polyfluorene with alkyl chains of consistently increasing length from H and methyl (CH_3) to dodecyl ($C_{12}H_{25}$).

We have focused on the effect of the alkyl length on the interplay between $\pi-\pi$ stacking and van der Waals alkyl-SWCNT interactions contributing to the PFO adsorption on the SWCNT surface and its chirality selectivity. Our calculations

DOI: 10.1021/acs.jpcc.9b04869
J. Phys. Chem. C 2019, 123, 24807−24817

show that the presence of side chains in PFO analogues results in an additional interaction through van der Waals forces that have a cumulative effect on the strength of adsorption to SWCNTs. Side chains longer than ethyl groups additionally have a significant role in changing the geometry of the wrapped polymer, resulting in decreased $\pi-\pi$ stacking and therefore reduced binding energy, while the optimal strength of interaction is achieved for octyl groups due to increased van der Waals interactions between the side chains and SWCNTs. Our simulations also confirm that the selective interactions of PFO chain with a particular nanotube chirality takes place only for long alkyl groups starting with octyl groups and longer, while $\pi-\pi$ stacking is not capable of providing chirality sensitive interactions.

Due to the large number of atoms in a unit cell of a SWCNT governing the relatively high computational expense, computational studies of the electronic structure and optical response of noncovalently functionalized SWCNTs are limited in number.[31] To reduce computational expense, single-point density functional theory (DFT) based studies can be carried out on systems with reliable geometries. As such, a prerequisite to accurate electronic structure is determination of the geometry of the systems, which can be obtained by lower level theory requiring less computationally resources, such as MM3 force field, which we have applied in our studies. Our calculations confirm that alkyl side groups should not be reduced or substituted by H or CH_3 groups for studies where the strength of binding of such an adsorbent to a SWCNT is concerned, and inclusion of the effect of the side chains is required to accurately model the structure of SWCNTs functionalized by conjugated polymers.

1. METHODOLOGY

In order to accurately model the SWCNT-PFO system-specific geometry using MD, we first re-parametrized the MM3 force field. This was accomplished by optimizing the geometry of an oligomer of PFO composed of five monomers with side groups substituted with methyl groups (m = 5, total length 41.4 Å) in vacuum, Figure 1. First, calculations were performed using DFT, as implemented in Gaussian09 software.[52] We used the B3LYP[53−55] functional and 6-31G* basis set,[56−58] which is a common methodology applied in simulations of various conjugated polymers.[59] Alkyl chains were replaced with methyl groups (n = 1), an accurate approximation due to the lack of a significant effect of side chains on either the geometry of the backbone in the pristine polymer or its electronic structure, especially when the side groups are spaced as distantly as possible to minimize steric effects.[31,60]

Following the procedure reported in literature,[60,61] we reparameterized the height and the shape of the torsional barrier parameters of MM3−2000 force field[62−65] to match the B3LYP-dependence of the total electronic energy on the torsional angle between two central fluorene units in the isolated PFO oligomer (Figure 1c), as well as the bond length between two sp^2 hybridized carbons in five membered rings. The modified parameters are available in the Supporting Information (SI), Figure S1 and Tables S1 and S2. The modified MM3−2000 force field is then used for geometry optimization of PFO molecules with various length of alkyl groups and SWCNTs functionalized by these PFO chains utilizing Tinker software package.[66] This force field introduces van der Waals forces through a set of parameters accurately describing the packing of crystals of alkanes and simple aromatics[64] and therefore is sufficient to describe the same interactions in our systems. All calculations are performed in vacuum. The vacuum calculation is valid due to the nonpolar character of PFO-SWCNT systems that are typically dispersed in nonpolar organic solvents, where dipole−dipole interactions are negligibly small. As such, embedding the system to a weakly polar media is not expected to be efficient for solvent simulations in this case.

Twelve SWCNTs of various chiralities were generated using Tubegen software.[67] A single monomer of the PFO with alkyl side groups having n number of carbon atoms arranged linearly in each side chain—systematically varying from n = 0 (alkyls are substituted by hydrogens) to n = 12 (Figure 1a)—was then placed parallel to the SWCNT surface at the distance of 3.3 Å from the SWCNT. Such a placement was chosen to reproduce the favorable conditions for the $\pi-\pi$ stacking between PFO backbone and the SWCNT, which are expected to be the primary interaction governing the polymer-SWCNT binding. This monomer unit was then replicated and placed head-to-tail to create a polymer chain 40 units long. Following the procedure[25,31,68] used for creating initial structures of DNA-wrapped and PPV-wrapped SWCNTs, the replicated monomer units were placed at some angle with respect to the SWCNT axis representing PFO wrapping about the SWCNT at various angles of 0° to 80° in 10° increments. As such, nine initial configurations were generated for each SWCNT-PFO system in order to reproduce the random geometries that are typically generated by more computationally expensive MD simulations, an approximation that was implemented in numerous previous studies.[30,36,40−47]

We validate our simplified approach by performing 500 ps MD simulations at room temperature sampling the potential energy surface (PES) of a vast number of plausible morphologies of PFO with side chains of n = 8 and n = 10 to the (8,7) SWCNT (see technical details in SI). The results of the MD simulations largely agree with the results from the optimization, Figures S2−S6 in the SI. Analyzing the Boltzmann means for each morphological parameter, we recover the trends portrayed in the optimization results. The outcomes of MD simulations (Figures S2 and S3 in the SI) demonstrate that local energy minima are separated by energy barriers of significant enough magnitude that they are unable to be overcome by thermal energy, as illustrated in Scheme 1. Our approach of generating a number of starting geometries distinct in wrapping angles and then optimizing each is therefore a valid approach for finding the

Scheme 1. Energy Landscape with Respect to the Wrapping Angle of the PFO over the SWCNT[a]

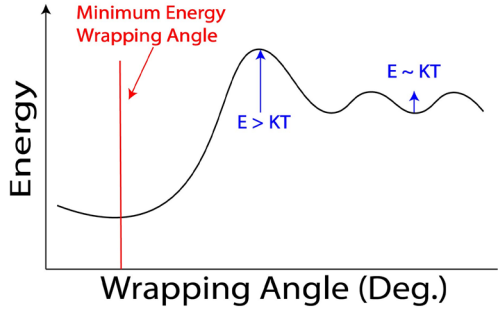

[a]The energy varies in smooth manner at lower angles, while the structures with larger wrapping angles are well separated by a large energy barrier, which is not to be overcome by thermal energy.

DOI: 10.1021/acs.jpcc.9b04869
J. Phys. Chem. C 2019, 123, 24807−24817

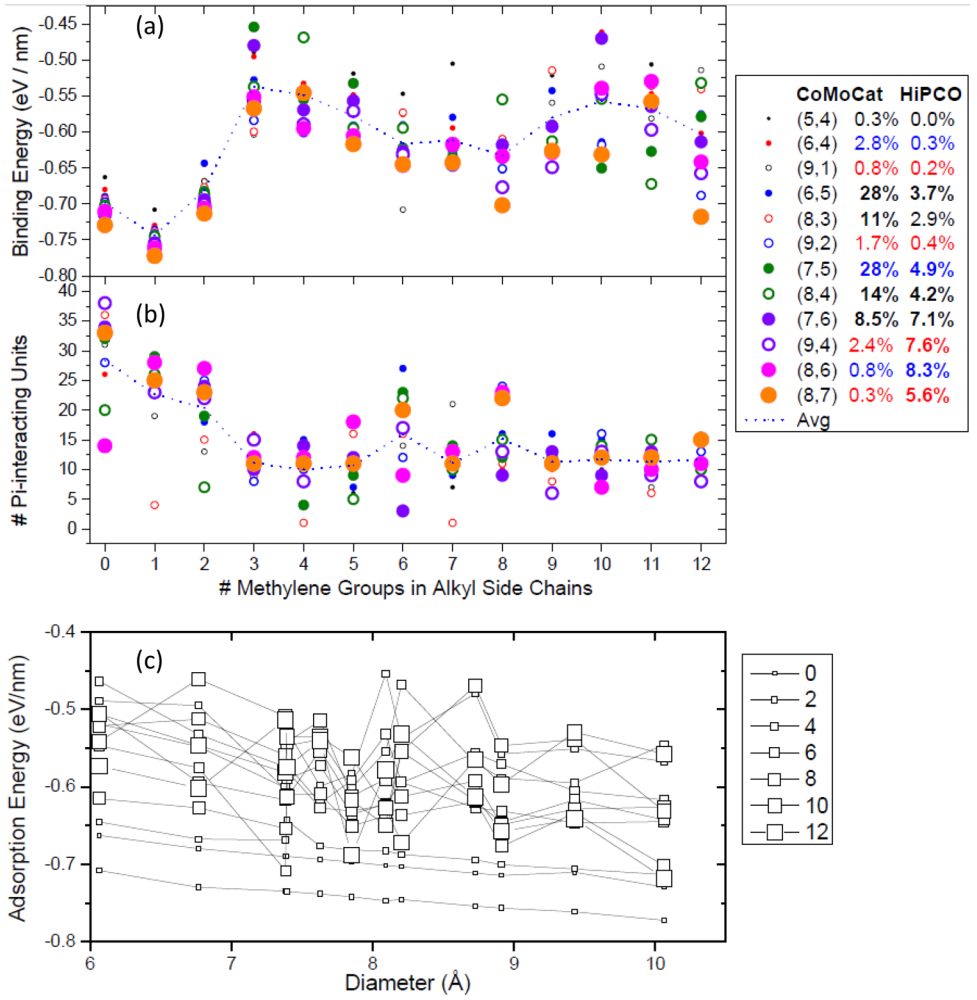

Figure 2. (a) SWCNT-PFO adsorption energies per unit length of PFO. (b) The number of PFO units that are both planar to the surface and have all backbone C atoms within distance range of $\pi-\pi$ stacking as a function of number of methylene groups in the alkyl chain. The right panel identifies tube chiralities and the relative chirality population of SWCNT samples prepared using CoMoCat and HiPco methods, as reported in refs 50 and 51. Bold font highlights chiralities that are the most present in samples (>3%) according to ref 70. The red font identifies chiralities with the lowest adsorption energy (<−6.5 eV/nm) and the blue font depicts species having adsorption energies close to the averaged energy (−0.62 eV), as calculated for PFO with octyl groups. Filled circles indicate species with tube's chiral angles $\theta > 20°$ and empty circles indicate $\theta < 20°$. The size of circles correlates with the tube diameter. (c) SWCNT-PFO adsorption energy as a function of the SWCNT diameter. The size of squares correlates to the length of the alkyl side chain of PFO: the larger a squire, the longer the alkyl group (larger n).

most stable conformations that are representative in experimental samples.

The generated PFO-wrapped SWCNT geometries were optimized by Tinker software using the reparameterized MM3 force field. This was accomplished in two steps: first by freezing the SWCNT and relaxing the geometry of the polymer about the tube; second, relaxing both the SWCNT and polymer and allowing the system to relax to its final geometry. This two-step procedure was used to better optimize initially high forces in the PFO-wrapped SWCNT geometries. With the geometry of the entire system determined, the adsorption energy (E_{ads}) of the polymer to the SWCNT was calculated for all geometries using the following equation:

$$E_{ads} = E_{SWCNT\text{-}PFO} - (E_{SWCNT} - E_{PFO}) \quad (1)$$

where $E_{SWCNT\text{-}PFO}$ is the total energy of the SWCNT-PFO system, E_{SWCNT} is the energy of the optimized pristine SWCNT, and E_{PFO} is the energy of the isolated 40 unit long PFO chain optimized from the 0° wrapping configuration. This geometry was chosen to eliminate the energy contributions arising from intramolecular interactions between distant PFO units.

The most stable SWCNT-PFO conformations with the most negative value of the adsorption energy was then characterized based on its morphological parameters, including the average distance between the SWCNT and the carbon atoms of the sp^2 hybridized PFO backbone, the average distance between the SWCNT and the sp^3 hybridized atoms of the side chain, the final wrapping angle of the PFO chain about the SWCNT, and the torsion angle between PFO units in the polymer. From this data, the fraction of carbon atoms in the side chain interacting with the SWCNT via van der Waals interactions was defined as the number of carbon atoms in alkyl groups that were within a 4.5 Å distance from the surface of the SWCNT divided by the total number of carbons in alkyl side group.

Additionally, a further morphological parameter of the systems was defined as the "twisting" parameter to identify the contribution of the $\pi-\pi$ stacking to the interaction between the SWCNT and the PFO backbone. For this parameter, a vector normal to each monomer unit within the polymer was defined.

DOI: 10.1021/acs.jpcc.9b04869
J. Phys. Chem. C 2019, 123, 24807−24817

The minimum distance between this vector and the axis of the SWCNT was then determined and divided by the distance between the center of mass of the monomer unit and the axis of the SWCNT. As such, the possible range of the twisting parameter ranges from zero to one, where a value of zero suggests the unit is aligned perfectly parallel on the surface of the SWCNT and, thereby, maximizes $\pi-\pi$ overlap, while a value of one implies the monomer unit is aligned completely perpendicular to the surface of the SWCNT and, thereby, minimizes $\pi-\pi$ stacking, as illustrated in Figure 1b. Utilizing the measure of distance between the sp^2 hybridized fluorene backbone atoms and the SWCNT together with the twisting parameter, the number of monomer units in the PFO that are expected to interact via $\pi-\pi$ interactions was determined. For this, it was assumed that the unit interacts via $\pi-\pi$ stacking if the distance between every atom in the fluorene monomer (excluding side chains) and the SWCNT surface is less than 4 Å and the twisting parameter is less than 0.4. As such, the number of $\pi-\pi$ units in each PFO-SWCNT system is determined as the number of fluorene units that are both parallel to the surface of the SWCNT surface and within the distance expected for $\pi-\pi$ stacking.

2. RESULTS AND DISCUSSION

The profile for the adsorption energy of the PFO 40-mer with alkyl chains of varying length to SWCNTs of different chiralities is shown in Figure 2. It has a complex trend and exhibits several well-defined local minima for systems with methyl (n = 1) and octyl (n = 8) side groups, and less pronounced minima for hexane (n = 6) and dodecane (n = 12) groups, Figure 2a. Overall, the profile of the average adsorption energy as a function of the alkyl length well correlates with those for the number of $\pi-\pi$ stacking units in the PFO backbone, Figure 2b. With the exception of a few deviations, a greater the number of fluorene units contributing to the $\pi-\pi$ interactions between the PFO backbone and the SWCNT surface results in a more stable the PFO-SWCNT structure. This correlation elucidates the dominating role of the $\pi-\pi$ stacking in the stabilization of the PFO-SWCNTs composites.

However, there are several deviations from this trend: (i) n = 1 shows an absolute minimum in the average absorption energy, but not the maximal average number of $\pi-\pi$ stacking units, and (ii) for n > 8, the average number of $\pi-\pi$ stacking units is nearly constant (about 11−12 units), while the average absorption energy has a well pronounced maximum for n = 10 and a minimum for n = 12. These discrepancies suggest non-negligible contributions of side alkyl chains, especially when they are long enough, which agrees with conclusions from previous reports.[32,33]

In average, the adsorption energy varies from −0.78 eV to −0.45 eV per polymer length, demonstrating strong polymer−nanotube interactions governing formation of relatively stable PFO-SWCNT composites for many tube chiralities. The estimated PFO-SWCNTs interactions are stronger than those calculated[31] between PPV polymers and SWCNTs and comparable to the DNA-SWCNT interactions.[25,68] More stable character of PFO-SWCNT versus PPV-SWCNT composites originates from a larger size of the conjugated unit of PFO compared to those of PPV, which provides better conditions for the $\pi-\pi$ stacking. The same effect compensates for the dipole interactions taking place in DNA-SWCNT structures, making interactions between the DNA bases and SWCNTs comparable to those of PFO and SWCNT, despite the nonpolar character of PFO molecules.

In the case of very short side chains (n < 4), the adsorption energy shows a very distinct trend with the nanotube diameter: The polymer-SWCNT interaction linearly increases with the nanotube diameter, Figure 2c. This trend is mainly governed by the $\pi-\pi$ stacking between the PFO backbone and the π-conjugated rings in the SWCNT (Figure 2b), facilitated by the larger nanotube surface providing better conditions for the $\pi-\pi$ overlap. This trend is smooth resulting in a change of PFO-SWCNT binding energy of not more than 0.05 eV comparing tubes with the diameter of about 0.6 nm to about 1 nm and a further reduction (<0.01 eV) for nanotubes in the range of 0.8−1.1 nm. As such, the diameter selectivity is limited for small-diameter SWCNT species to PFO with short side chains. In contrast, for longer alkyl groups, the dependence on the diameter becomes complicated showing many deviations from the linear trend, with significant variations in adsorption energy up to 0.3 eV. This implies that increase in the length of the side chain likely leads to many distortions and a strong disorder in the PFO backbone alignment with respect to the tube surface, which brings randomness in PFO-SWCNT interactions, while providing conditions for selective interactions with a particular SWCNT type.

Trends in selective adsorption to the specific chiral angle of the SWCNT are not pronounced for short side chains (n < 4), having insignificant changes in adsorption energies (<0.05 eV) between various chiralities. However, the variations in the PFO-SWCNT adsorption energy for different chiralities noticeably increases for side chains with n > 3 (Figure 2a) and becomes significant (up to 0.1−0.3 eV) to govern chirality selective binding for $n \geq 8$, which agrees with experimental findings.[32,39] In particular, it was experimentally shown that the standard PFO with octyl groups (PFO8) enables the generation of SWCNT dispersions containing exclusively (7,5), (8,6), and (8,7) nanotubes with diameters less than 1.2 nm.[32,33,69] At first glance, our computational data disagrees with these experimental findings, providing significantly stronger PFO8-SWCNT interactions (E_{ads} < −0.65 eV) for (8,7), (9,4), (9,1), and (9,2) SWCNTs that are distinct from other chiralities (Figure 2a, marked by red) and relatively stable composites of (7,5), (8,6), and (6,4) SWCNTs with $E_{ads} \approx -0.62$ eV close to the adsorption energy averaged over all chiralities (Figure 2a, marked by blue).

However, one needs to take into consideration nonequal distribution of chiralities in SWCNT samples prepared by HiPCO and CoMoCat methods, as has been estimated from the relative fluorescence intensities of various SWCNTs chiralities in PFO-free samples.[70] If we eliminate the chiralities that have less than 3% of fluorescence intensity due to their population scarcity, then selectively stable PFO8-SWCNT structures take place for (7,5), (8,6), (8,7), and (9,4) SWCNTs in HiPco samples and predominantly for (7,5) in CoMaCat samples, which agrees well with literature reports,[32,33,39,69] except for (9,4) SWCNT. But even for (9,4) nanotube, there are no direct contradictions with experiments, since it was shown that selectivity over chiralities in PFO8-SWCNT samples is sensitive to the solvent:[33,39] Changing toluene to THF results in stronger selectivity of PFO8 toward the (9,4) SWCNT.[33] Our calculations demonstrate that increasing the alkyl length from n = 8 to n = 12 slightly rearranges the adsorption energy of the stable conformations, while (8,7), (8,6), (7,5), and (9,4) mainly stay predominantly stable over other abounded chiralities, but

DOI: 10.1021/acs.jpcc.9b04869
J. Phys. Chem. C 2019, 123, 24807−24817

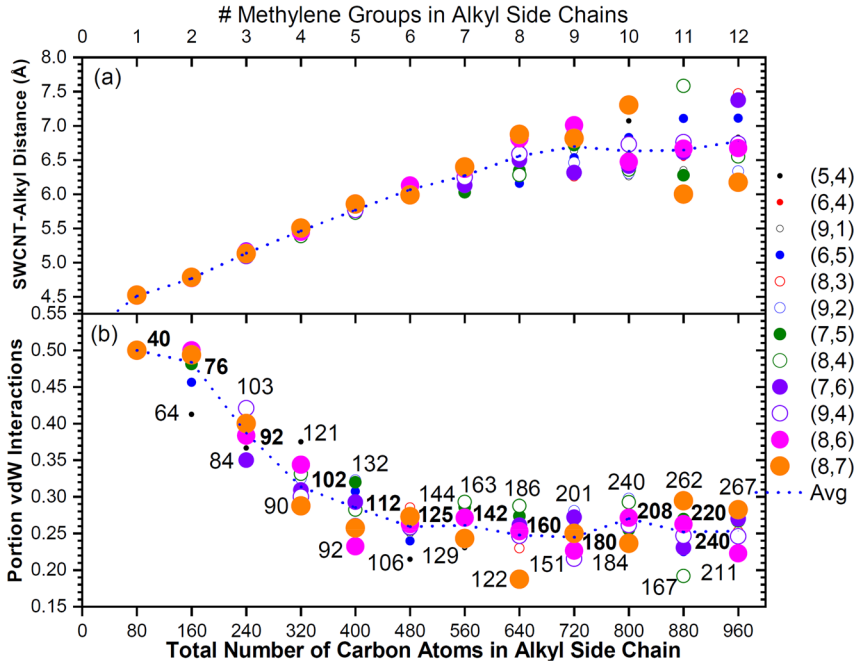

Figure 3. Characterization of the interaction of the PFO side chains with the SWCNT surface. The average distance between the SWCNT atoms and the atoms of the PFO alkyl group (a) and the portion of carbon atoms in the alkyl group that are within the range of optimal van der Waals interactions with the SWCNT (b) as a dependence on the alkyl length. The size of circles in correlates with the nanotube diameter: the larger a circle, the larger diameter; filled circles indicate a nanotube chiral angle $\theta > 20°$, and empty circles indicate $\theta < 20°$. The values in (b) identify the minimal, maximal, and average over tube's chiralities (a bold font) number of carbons belonging to all alkyl chains and contributing to the van der Waals interactions.

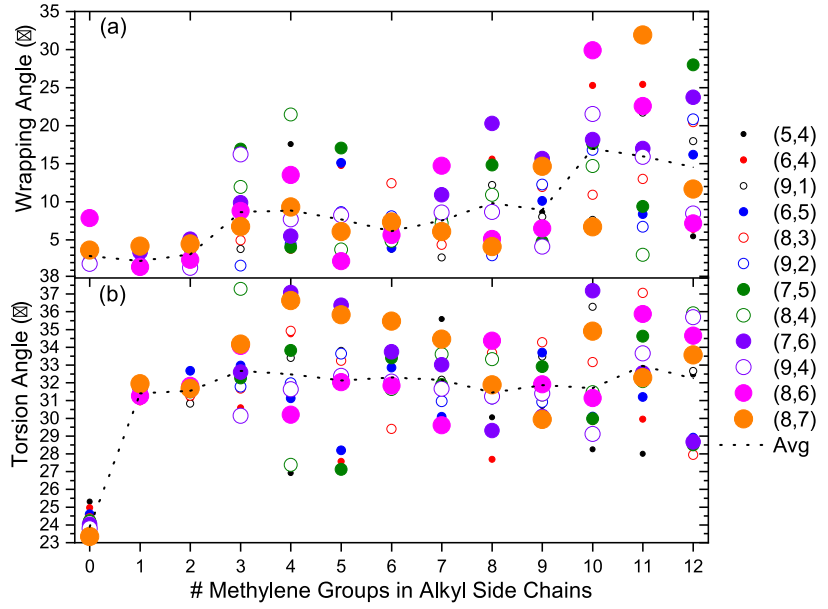

Figure 4. Characterization of the geometry of the PFO polymer optimized in the presence of the SWCNT. (a) The average wrapping angle of the PFO and (b) the average torsion angle between polymer units, as a function of alkyl length. The size of circles correlates with the nanotube diameter: the larger a circle, the larger diameter; filled circles indicate a nanotube chiral angle $\theta > 20°$, and empty circles indicate $\theta < 20°$. While wrapping angle shows increase with the alkyl length, the torsion angle of PFO is not as sensitive to the alkyl groups, except when alkyls are substituted by hydrogens ($n = 0$).

extending to (8,4) ($n = 11$) and (7,6) ($n = 12$), which also agrees with experimental data.[32] Overall, the correlations between results from our calculations and previous experimental and computational studies validate our approach.

Our main goal is to determine to what extent the van der Waals interactions between the SWCNT and the side alkyl groups complement the $\pi-\pi$ stacking in stable PFO-SWCNT composites and identify the main mechanisms defining the chirality-selective abilities of PFO and their side groups. For this, we systematically analyze the geometrical parameters characterizing the interaction of the PFO side chain with the SWCNT, as presented in Figure 3, and compare to the contributions of the PFO backbone, Figure 2b and SI Figure S7. Surprisingly, the PFO-SWCNT systems with hydrogen side groups (n = 0, PFO0) show weaker polymer-SWCNT interactions ($\Delta E_{ads} \approx$ 0.06 eV) than those of methyl groups (n = 1, PFO1), while

DOI: 10.1021/acs.jpcc.9b04869
J. Phys. Chem. C 2019, 123, 24807−24817

demonstrating the maximal average number of $\pi-\pi$ stacking units (about 30 from 40, in average) contributing to the $\pi-\pi$ interactions between the PFO0 backbone and the SWCNT, as well as the smallest average distance ($\leq$3.4 Å) between the PFO0 units and the nanotube, SI Figure S7.

This points to a key contribution of the methyl groups via van der Waals interactions compensating for the slight decrease in the $\pi-\pi$ interactions between the PFO1 backbone and the SWCNT (23 units in average, varying from 5 to 30 units depending on the tube's chirality, Figure 2b). Relatively strong van der Waals interactions in the case of methyl groups originate from the ordered alignment of the PFO1 on the nanotube surface. In fact, exactly half of the methyl groups are located directionally toward the SWCNT surface (structures are illustrated in SI Figure S8) and, therefore, fall within the optimal van der Waals interaction distance (~4.5 Å, Figure 3). Such an ordered alignment is a result of increased torsion angles (~32°) in the PFO1 backbone, compared to 24° in PFO0 adsorbed on SWCNTs (see Figure 4), with the latter dictated by reduced steric hindrance due to the absence of side chains in PFO0.

Note that further increase in alkyl length from n = 1 to n = 12 insignificantly changes the average torsion angle, while only increases the fluctuations in its values from 28° to 37°, depending on the tube chirality, Figure 4. Larger torsion angles make the PFO1 backbone less planar than those of PFO0, which results in tilting each second methyl group closer to the SWCNT surface, while the other half on opposite sides of the fluorene-backbone are directed away from the SWCNT and do not contribute to PFO1-SWCNT interactions. The cumulative effect of the additional van der Waals interactions brought by 40 methyl groups (Figure 3b) contributes about 0.05 eV to the adsorption energy, stabilizing these structures compared to those with only hydrogen atoms for all considered nanotube chiralities.

However, for systems with n = 1 to n = 3, the strength of the PFO-SWCNT interaction rapidly decreases by about 0.2 eV reaching its minimal interaction at n = 3, Figure 2a. This destabilization of structures with short alkyl chains ($1<n<4$) is induced by a significant twisting of the polymer backbone with respect to the SWCNT, so that many of fluorene conjugated units are not parallel to the nanotube surface, Figure 1d. This trend is supported by the increased twisting parameter (from 0.3 to 0.5) and the average SWCNT-backbone distance (from 3.38 to3.65 Å), Figure S7 in SI. As a result, $\pi-\pi$ stacking is significantly disrupted in PFO-SWCNT structures with $n \geq 3$ resulting in the average number of $\pi-\pi$ units less than 15, Figure 2b. The morphology of systems with the side chains consisting of 2 to 3 methylene groups is much less ordered than for SWCNT-PFO1 with methyl groups. Some fluorene units exhibit the alkyl chain interacting with the SWCNT while many other do not, which increases the average distance between the SWCNT and carbons in side groups with alkyl length, Figure 3a. Note that the same trend in the alkyl-SWCNT distance due to the high degree of the structural disorder is also observed for systems with n > 4, leading to a raise in the average distance between the SWCNT and side groups with the alkyl length, despite the overall growth of the number of atoms interacting through van der Waals forces, Figure 3.

Contrary to the behavior of structures with methyl groups, many units with n = 3 have the side chains on both sides of the polymer backbone interacting with the SWCNT, as illustrated in SI Figure S9. This alignment of side groups increases the number of their atoms interacting through van der Waals interactions (Figure 3b) while inducing complete disruption of $\pi-\pi$ stacking. However, the increase in van der Waals interactions as a result of the additional atoms in the alkyl side chain is insufficient to offset the corresponding decrease in the portion of $\pi-\pi$ interacting units (~1/4 of all units in average, Figure 2b) as a result of twisting. The net effect is a significant destabilization of the adsorption energy between the SWCNT and PFO with increased number of methylene groups from 1 to 3 in side chains.

The average twisting parameter of the polymer backbone reaches a maximum for systems with n = 3, and further twisting in the backbone is not as pronounced with increasing length of the side chain, SI Figure S7, so that the average number of $\pi-\pi$ units slightly fluctuating between 10 to 15 units with alkyl length growing from n = 3 to n = 12. For systems with n = 3 to n = 5, the average number of $\pi-\pi$ units stays nearly the same (~10 units), while the average SWCNT-backbone distance slightly decreases (from 3.65 E to 3.60 E, Figure S7 in SI), increasing the strength of $\pi-\pi$ interactions. In addition, the number atoms in side groups interacting via van der Waals interactions also slightly increases by about 10 atoms in average, Figure 3b. As such, going from n = 3 to n = 5, the net result is a stabilization of the SWCNT-PFO adsorption energy ($\Delta E_{ads} \approx$ 0.05 eV, Figure 2a) through both the slightly increased strength in alkyl-SWCNT van der Waals and $\pi-\pi$ interactions.

For n = 6 and n = 8, the number of $\pi-\pi$ units increases from 10 to 15 (up to 1/3 of all PFO units), facilitating the $\pi-\pi$ stacking, which results in a significant stabilization of the adsorption energy. However, the energy stabilization of structures with octyls is more pronounced due to the drastically increased number of interacting atoms from side groups (~40 atoms more than in n = 6, Figure 3b). In the case of n = 8, the increased number of atoms interacting through van der Waals forces originates from the interacting alkyl chains that belong to the same fluorene unit and are long enough to "hug" the SWCNT, as depicted in Figure 1e. Note that chiral species with the strongest SWCNT-PFO8 interactions, in particular (8,7), are the most distinct toward increased number of both $\pi-\pi$ units and alkyl-SWCNT van der Waals interactions, providing their selectivity among other chiralities.

Interestingly, with alkyl length increasing from n = 6 to n = 12, the average fraction of interacting sp^3-hybridized carbons of alkyls with sp^2-hybredized carbons of SWCNTs reaches its saturation at about 0.25 of the total number of carbon atoms in the side chains. This saturation is likely dictated by the steric repulsions between long alkyl groups at the adjacent units, so that only 25% of alkyl atoms can come in a sufficient proximity to the SWCNT for van der Waals interactions. However, since the total number of atoms raises with the alkyl length, the absolute number of van der Waals interacting atoms noticeably increases, growing by about 20 atoms with increase of n from 6 to 12, Figure 3b. Overall, this agrees with the maximum coverage model proposed for SWCNT wrapped in P3HT polymers.[47]

Despite an increase in van der Waals interactions due to the contributions of side groups, the number of $\pi-\pi$ interacting units drops from 15 units to 11−12 units, in average, when the polymer alkyl chains are lengthened beyond octyl groups. This results in destabilization of the SWCNT-PFO adsorption energy for systems with n > 8, Figure 2a. The largest destabilization is achieved at n = 10, which is mainly governed by increase in the average SWCNT-backbone distance (reaching its threshold value of 3.8 Å, SI Figure S7) and results in the reduced strength of $\pi-\pi$ interactions. In the case of n = 10, increase in the alkyl-

DOI: 10.1021/acs.jpcc.9b04869
J. Phys. Chem. C 2019, 123, 24807−24817

SWCNT van der Waals interactions is not sufficient to compensate a decreased strength of the $\pi-\pi$ interactions. However, for systems with $n > 10$, the average SWCNT-backbone distance slightly reduces (~3.7 Å), so that increase in the van der Waals interacting atoms is capable for the net increase in the SWCNT-PFO interactions, stabilizing the adsorption energy by about 0.05 eV for $n = 12$, compared to $n = 10$.

It is important to note that a distribution in the number of $\pi-\pi$ interacting units with the nanotube's chiralities is less pronounced for long alkyl groups with $n > 8$ (varying from 5 to 17 units), compared to systems with $n < 8$ (varying from 5 to 30 units), with the largest fluctuations observed for $n < 3$ (varying from 5 to 38 units), Figure 2b. In contrast, the variations in the number of alkyl-SWCNT van der Waals interacting atoms for different nanotube's chiralities consistently increases with alkyl length with a change from 5 to 20 atoms for $1 < n < 4$ and from 50 to100 atoms for $n > 8$, depending on the chirality, Figure 3b. Comparing these trends to chirality driven distributions in the SWCNT-PFO adsorption energies, we can conclude that chirality selective interactions are mainly governed by van der Waals interactions between the SWCNT and the PFO with long alkyl groups ($n \geq 8$). In contrast, the $\pi-\pi$ stacking results in less selective interactions between the PFO with short side groups and specific nanotube types.

This behavior correlates with the trend in increasing of the wrapping angle of the polymer with the alkyl length, Figure 4a. For PFO with $n < 3$, the average value of the polymer wrapping angle slightly fluctuates around 5°, showing negligible changes with nanotube chirality. For these structures, the $\pi-\pi$ interaction dominates with insignificant dependence on the tube chirality. For systems with the alkyl length ranging from $n = 4$ to 8, the wrapping angle averages to ~10°, exhibiting marginal variations (from 3° to 20°) with the chirality of SWCNT. For PFO8, the calculated wrapping angles at the range of 10° exhibits reasonable agreement with experimental measurements of 12°, 17° and 14° ± 2° for the highly selected (7,5), (8,6), and (8,7) species.[69] Remarkably, our MD simulations of (8,7) SWCNT wrapped in PFO8 also predict the most stable structures for the wrapping angle at the range of 10°−13°, which are separated by a significant energy barrier ($\gg kT_{room}$) from structures with the wrapping angles larger than 14°, Figures S2 and S3.

It is important to note that PFO-SWCNT dispersions can be heterogeneous in nature with multiple PFO oligomers/polymers interacting with one another and the SWNT.[32,33] However, well-resolved wrapping angles reported in ref 69, together with the observations of the best chirality sorting at low PFO concentrations during ultrasonication, at which the PFO strands become more ordered on the SWCNT surface and the surface coverage is low, point to a high probability of having structures with a single PFO chain wrapped around the SWCNTs. Our MD and optimization calculations do not detect PFO−PFO self-interactions for the most stable wrapping geometries. Such a trend is rationalized by much weaker PFO−PFO interactions, compared to interactions between the PFO and SWCNTs that are facilitated by a large surface area of the nanotube.

When the side alkyl chains are lengthened beyond octyl groups, a significant increase in the wrapping angle is observed, accompanied by large variations from 5° to 35° depending on nanotube chirality, Figure 4a. The elongation of the side chains increases the steric repulsions between alkyl groups on the adjacent units. Aligning the polymer circumferentially along the SWCNT at larger wrapping angles allows for retention of the torsion angle within the fullerene units while affording a greater volume in space for the alkyl groups to occupy, minimizing steric repulsions. However, increasing the wrapping angle to more than 15° results in an overall decrease of SWCNT-PFO adsorption energy, while large variations in wrapping angles facilitate the chiral selectivity of PFO with long alkyl groups, SI Figures S10 and S11. This trend of rapid destabilization of PFO/SWCNT conformations with increase in the wrapping angles is also confirmed by the MD simulations for a larger ensemble of (8,7) nanotubes with PFO8 and PFO10, SI Figures S2 and S3.

Understanding the role of the wrapping angle of the polymer with respect to the tube axis and possible correlations between this angle and the tube chirality might provide guidance for rational synthesis of the polymer isomers that favor certain wrapping angles. In fact, previous joined experimental and computational studies[30] elucidated that 2,7-isomers of oligocarbazoles tend to gradually coil around the entire tube, while 3,6- and mixed 2,7−3,6-oligocarbazoles irregularly bunch together on one side of the tube, due to their "zigzag" wrapping geometry. Such localization of oligocarbazoles containing 3,6-isomers on one side of the nanotube prevents tube unbundling, and leads to photoluminescence quenching in SWNTs, while 2,7-oligocarbazoles exhibit well-resolved emission.

The optimization of two identical pristine SWCNTs placed at the distance of 3.2 Å that is typical for $\pi-\pi$ stacking, results in averaged binding energy between the tubes of −1.08 eV/nm, while the final distance between tubes stays of ~3.2 Å. These results confirm a strong interaction between nanotubes that make small bundles of nanotubes very stable. The obtained SWCNT-SWCNT interaction is stronger than the PFO-SWCNT interaction even for the most stable composites (−0.73 eV/nm). This is expected since the nanotubes interact via the perfect $\pi-\pi$ stacking along their entire length, while PFO has a lot of destructions in the $\pi-\pi$ stacking especially for long alkyl groups, where only ~1/3 conjugated units of the PFO oligomer contribute to the $\pi-\pi$ interactions. However, this difference in the binding energy does not mean that PFO is not capable for tube unbundling. In experimental samples, tub's bundling is overcome by sonication in a solution containing the PFO polymer that acts as a surfactant. The result is individual SWCNTs covered with the surfactant polymers. Once the SWCNTs are dispersed and wrapped by the PFO, the polymer-SWCNT interaction does not necessarily need to be stronger than the SWCNT-SWCNT interactions for the stable SWCNT/PFO systems, because the PFO wrapping around the nanotube does not allow other tubes to come close enough to initiate $\pi-\pi$ stacking. The PFO wrapping angle of 10°−15° provide additional stabilization of the PFO-SWCNT composites, since conjugated structures placed nearly parallel to the tube surface can be easily removed due to the thermal and mechanical motion of composites in the solvent during sonication, compared to the structures where polymers are helically wrapped around the tube. This is confirmed by our MD simulations, demonstrating slightly higher averaged wrapping angles (~10°) for the ensemble of (8,7) nanotubes wrapped in PFO8 and PFO10 at 298 K, compared to the results of the optimized structures at 0 K (~5°), as can be compared in Figures 4a and S2, and S3.

Our calculations also reveal that nearly perfect $\pi-\pi$ stacking provided by short side groups (H or CH_3) is not capable for selective binding with respect to the tube's chiralities, resulting

DOI: 10.1021/acs.jpcc.9b04869
J. Phys. Chem. C 2019, 123, 24807−24817

in the energy difference between different tubes less than 0.1 eV/nm. This contradicts to the common idea that the selective binding to specific tube's chirality is expected to originate from the best $\pi-\pi$ orbital overlaps between the aromatic rings of the polymer and the SWCNT.[25] In fact, such trends have been observed in SWCNTs wrapped by a single strand DNA, depending on the DNA sequence.[26,68] However, our calculations demonstrate that at nearly perfect $\pi-\pi$ stacking between PFO and SWCNTs, the polymer wrapping does not correlate to the tube chirality and the most stable wrapping angle is ~5°, with small variations by ±3° between tube chiralities (see Figure 4). As such, PFO-SWCNT $\pi-\pi$ stacking does not differentiate between different tube chiralities and is not responsible for their selectivity. This also means that the mechanism of selective binding to specific tube chiralities is different between DNA and conjugated polymers.

3. CONCLUSIONS

In this study, we have revealed the effects of the length of alkyl side chains on PFO's binding to narrow SWCNTs within the diameter range of 0.6 nm −1.1 nm. The adsorption strength of PFO is highly dependent on the length of their alkyl side chains, while follows complicated dependence governed by the interplay between the $\pi-\pi$ stacking and van der Waals interactions. Our calculations clearly show that the additional van der Waals interaction with the SWCNT afforded by methyl side chains noticeably strengthens the interaction with the nanotube. However, as the chain elongates, steric repulsion begins to take effect resulting in the twisting of the polymer backbone and therefore destruction of the $\pi-\pi$ stacking. This results in weaker PFO-SWCNT binding despite the additional contributions of alkyl-SWCNT van der Waals interactions. Maximal twisting in the polymer backbone is observed for the propyl side chain (n = 3), while further elongation leads to stabilization of the binding energy due to the additional van der Waals interactions that become large enough to compensate for decreased $\pi-\pi$ interactions. A local maximum in interaction strength is obtained for octyl chains (PFO8), with the relative prevalence of (7,5), (8,6), (8,7), and (9,4) SWCNTs in HiPco samples and (7,5) in CoMaCat samples. These computational results justify the relative ease by which these species can be isolated in experiment using PFO8 and its derivatives with longer side groups.

Overall, our calculations complement previous studies, as we explore the effect of alkyl chain lengths on small-diameter nanotubes with a large distribution in their chiralities. Such species coexist in experimental samples synthesized with the widely used HiPCO and CoMoCat methods, while previous computational studies have been focused on a limiting number of chiralities and larger diameter tubes.[32,33] We also provide important insights into the mechanism of the PFO-SWCNT interactions, which was missing in previous computations. In fact, our study contrasts the effects of van der Waals interactions between the SWCNT and the polymer side chains with the $\pi-\pi$ interactions between the SWCNT and the polymer backbone. Contrasting these interactions is of utmost importance because, as we demonstrate, one occurs at the expense of the others. This is a major conclusion of our report as it establishes the computational limitations of models neglecting side chains.

As a main result, we found that the length of the side groups governs the selective binding to specific nanotube chirality, while the PFO backbone units just provide stability of the polymer-SWCNT composite through $\pi-\pi$ interactions. Moreover, the van der Waals interactions between long side chains and SWCNT are maximized at the expense of $\pi-\pi$ interactions, resulting in overall weaker polymer-SWCNT binding. Despite the reduced $\pi-\pi$ interactions between the SWCNTs and PFOs with long alkyl groups having eight and more carbons in the side chain, the difference between the PFO binding energy to SWCNT species of different chiralities increases, providing favorable condition for selective binding.

Our calculations allow for establishing conditions for structures of SWCNT/PFO that favors selective binding. The stability of the SWCNT/PFO composite requires at least 1/3 of PFO conjugated units to contribute to the $\pi-\pi$ stacking, while alkyl groups should have eight or more carbons in the chain, but also poses reduced steric repulsion between side groups. These two conditions correlate with the requirement to the PFO wrapping angle with respect to the SWCNT axis being of less than 15 degrees. Such requirements are met only for a few tube chiralities interacting with PFO of a certain alkyl length. The obtained results suggest that chemical modification of the polymer units leading to increased $\pi-\pi$ stacking between the polymer and the SWCNT is not necessary to improve the chirality selectivity. Instead, modification of side groups of conjugated polymers to increase their van der Waals interactions with the SWCNT, while reducing their steric repulsions is expected to be promising toward selective binding to SWCNTs of specific chiralities.

■ ASSOCIATED CONTENT

Supporting Information

The Supporting Information is available free of charge on the ACS Publications website at DOI: 10.1021/acs.jpcc.9b04869.

Modified parameters for MM3−2000 force field; details on molecular dynamics simulations of (8,7) SWCNT wrapped in PFO with octyl and decyl side chain groups; analysis of sampling conformations obtained from MD simulations and comparison to those obtained from molecular mechanics optimization, including distance between the SWCNT and PFO backbone, number of $\pi-\pi$ interacting units in the PFO, distance between atoms contributing to van der Waals interactions between side alkyl groups and the SWCNT, and dependence of PFO-SWCNT binding energy on the PFO wrapping angle; and illustration of structures of SWCNT wrapped in PFO with methyl and propyl side groups (PDF)

■ AUTHOR INFORMATION

Corresponding Author

*E-Mail: svetlana.kilina@ndsu.edu.

ORCID

Brendan J. Gifford: 0000-0002-4116-711X

Braden M. Weight: 0000-0002-2441-3569

Svetlana Kilina: 0000-0003-1350-2790

Notes

The authors declare no competing financial interest.

■ ACKNOWLEDGMENTS

Authors acknowledge NSF Grant CHE-1413614 for financial support of studies of functionalized carbon nanotubes. For computational resources and administrative support, authors thank the Center for Computationally Assisted Science and Technology (CCAST) at North Dakota State University and the

DOI: 10.1021/acs.jpcc.9b04869
J. Phys. Chem. C 2019, 123, 24807−24817

National Energy Research Scientific Computing Center (NERSC) allocation awards 86678, supported by the Office of Science of the DOE under Contract No. DE-AC02-05CH11231. We also acknowledge the LANL Institutional Computing (IC) program for providing computational resources. This work was performed, in part, at the Center for Integrated Nanotechnologies and Center for Nonlinear Studies, Office of Science User Facilities operated for the U.S. Department of Energy (DOE) Office of Science by Los Alamos National Laboratory (Contract DE-AC52-06NA25396) and Sandia National Laboratories (Contract DE-NA-0003525).

REFERENCES

(1) Saito, R. *Physical Properties of Carbon Nanotubes*; Imperial College Press: 1998.
(2) Iijima, S. Helical microtubules of graphitic carbon. *Nature* **1991**, *354*, 56−58.
(3) Mintmire, J. W.; Dunlap, B. I.; White, C. T. Are fullerene tubules metallic? *Phys. Rev. Lett.* **1992**, *68*, 631−634.
(4) Dekker, C. Carbon nanotubes as molecular quantum wires. *Phys. Today* **1999**, *52*, 22.
(5) Nanot, S.; Thompson, N. A.; Kim, J.-H.; Wang, X.; Rice, W. D.; Hároz, E. H.; Ganesan, Y.; Pint, C. L.; Kono, J. Single-Walled Carbon Nanotubes. In Vajtai, R., Ed.; *Springer Handb. Nanomater.*; Springer Berlin Heidelberg: Berlin, Heidelberg, 2013: pp 105−146.
(6) Landi, B. J.; Raffaelle, R. P.; Castro, S. L.; Bailey, S. G. Single-wall carbon nanotube−polymer solar cells. *Prog. Photovoltaics* **2005**, *13*, 165−172.
(7) Lee, J. U. Photovoltaic effect in ideal carbon nanotube diodes. *Appl. Phys. Lett.* **2005**, *87*, 073101.
(8) Cataldo, S.; Salice, P.; Menna, E.; Pignataro, B. Carbon nanotubes and organic solar cells. *Energy Environ. Sci.* **2012**, *5*, 5919−5940.
(9) Zhang, D.; Ryu, K.; Liu, X.; Polikarpov, E.; Ly, J.; Tompson, M. E.; Zhou, C. Transparent, Conductive, and Flexible Carbon Nanotube Films and Their Application in Organic Light-Emitting Diodes. *Nano Lett.* **2006**, *6*, 1880−1886.
(10) Bansal, M.; Srivastava, R.; Lal, C.; Kamalasanan, M. N.; Tanwar, L. S. Carbon nanotube-based organic light emitting diodes. *Nanoscale* **2009**, *1*, 317−330.
(11) Chen, T.; Wei, L.; Zhou, Z.; Shi, D.; Wang, J.; Zhao, J.; Yu, Y.; Wang, Y.; Zhang, Y. Highly enhanced gas sensing in single-walled carbon nanotube-based thin-film transistor sensors by ultraviolet light irradiation. *Nanoscale Res. Lett.* **2012**, *7*, 644.
(12) Dhall, S.; Jaggi, N.; Nathawat, R. Functionalized multiwalled carbon nanotubes based hydrogen gas sensor. *Sens. Actuators, A* **2013**, *201*, 321−327.
(13) Zhang, T.; Nix, M. B.; Yoo, B.-Y.; Deshusses, M. A.; Myung, N. V. electrochemically functionalized single-walled carbon nanotube gas sensor. *Electroanalysis* **2006**, *18*, 1153−1158.
(14) Li, J.; Lu, Y.; Ye, Q.; Cinke, M.; Han, J.; Meyyappan, M. Carbon nanotube sensors for gas and organic vapor detection. *Nano Lett.* **2003**, *3*, 929−933.
(15) Zhang, W.-D.; Zhang, W.-H.Carbon nanotubes as active components for gas sensors*J. Sens.*2009*2009*
(16) Wang, Y.; Yeow, J. T. W. A review of carbon nanotubes-based gas sensors. *J. Sens.* **2009**, *2009*, 1.
(17) Liu, J.; Wang, C.; Tu, X.; Liu, B.; Chen, L.; Zheng, M.; Zhou, C. Chirality-controlled synthesis of single-wall carbon nanotubes using vapour-phase epitaxy. *Nat. Commun.* **2012**, *3*, 1199.
(18) Arnold, M. S.; Green, A. A.; Hulvat, J. F.; Stupp, S. I.; Hersam, M. C. Sorting carbon nanotubes by electronic structure using density differentiation. *Nat. Nanotechnol.* **2006**, *1*, 60−65.
(19) Ghosh, S.; Bachilo, S. M.; Weisman, R. B. Advanced sorting of single-walled carbon nanotubes by nonlinear density-gradient ultracentrifugation. *Nat. Nanotechnol.* **2010**, *5*, 443−450.
(20) Flavel, B. S.; Kappes, M. M.; Krupke, R.; Hennrich, F. Separation of single-walled carbon nanotubes by 1-dodecanol-mediated size-exclusion chromatography. *ACS Nano* **2013**, *7*, 3557−3564.
(21) Liu, H.; Nishide, D.; Tanaka, T.; Kataura, H. Large-scale single-chirality separation of single-wall carbon nanotubes by simple gel chromatography. *Nat. Commun.* **2011**, *2*, 309.
(22) Liu, H.; Tanaka, T.; Urabe, Y.; Kataura, H. High-efficiency single-chirality separation of carbon nanotubes using temperature-controlled gel chromatography. *Nano Lett.* **2013**, *13*, 1996−2003.
(23) Tanaka, T.; Liu, H.; Fujii, S.; Kataura, H. From metal/semiconductor separation to single-chirality separation of single-wall nanotubes using gel. *Phys. Status Solidi RRL* **2011**, *5*, 301−306.
(24) Zhang, H.; Wu, B.; Hu, W.; Liu, Y. Separation and/or selective enrichment of single-walled carbon nanotubes based on their electronic properties. *Chem. Soc. Rev.* **2011**, *40*, 1324−1336.
(25) Mayo, M. L.; Chen, Z. Q.; Kilina, S. V. Computational studies of nucleotide selectivity in dna−carbon nanotube hybrids. *J. Phys. Chem. Lett.* **2012**, *3*, 2790−2797.
(26) Yarotski, D. A.; Kilina, S. V.; Talin, A. A.; Tretiak, S.; Prezhdo, O. V.; Balatsky, A. V.; Taylor, A. J. Scanning tunneling microscopy of dna-wrapped carbon nanotubes. *Nano Lett.* **2009**, *9*, 12−17.
(27) Williams, R. M.; Nayeem, S.; Dolash, B. D.; Sooter, L. J. The effect of dna-dispersed single-walled carbon nanotubes on the polymerase chain reaction. *PLoS One* **2014**, *9*, No. e94117.
(28) Liang, Z.; Lao, R.; Wang, J.; Liu, Y.; Wang, L.; Huang, Q.; Song, S.; Li, G.; Fan, C. solubilization of single-walled carbon nanotubes with single- stranded dna generated from asymmetric pcr. *Int. J. Mol. Sci.* **2007**, *8*, 705−713.
(29) Zheng, M.; Jagota, A.; Semke, E. D.; Diner, B. A.; Mclean, R. S.; Lustig, S. R.; Richardson, R. E.; Tassi, N. G. DNA-assisted dispersion and separation of carbon nanotubes. *Nat. Mater.* **2003**, *2*, 338−342.
(30) Mayo, M. L.; Hogle, D.; Yilmaz, B.; Köse, M. E.; Kilina, S. Morphology and dispersion of polycarbazole wrapped carbon nanotubes. *RSC Adv.* **2013**, *3*, 20492−20502.
(31) Furmanchuk, A.; Leszczynski, J.; Tretiak, S.; Kilina, S. V. Morphology and optical response of carbon nanotubes functionalized by conjugated polymers. *J. Phys. Chem. C* **2012**, *116*, 6831−6840.
(32) Gomulya, W.; Costanzo, G. D.; de Carvalho, E. J. F.; Bisri, S. Z.; Derenskyi, V.; Fritsch, M.; Fröhlich, N.; Allard, S.; Gordiichuk, P.; Herrmann, A.; Marrink, S. J.; dos Santos, M. C.; Scherf, U.; Loi, M. A. Semiconducting single-walled carbon nanotubes on demand by polymer wrapping. *Adv. Mater.* **2013**, *25*, 2948−2956.
(33) Hwang, J.-Y.; Nish, A.; Doig, J.; Douven, S.; Chen, C.-W.; Chen, L.-C.; Nicholas, R. J. Polymer structure and solvent effects on the selective dispersion of single-walled carbon nanotubes. *J. Am. Chem. Soc.* **2008**, *130*, 3543−3553.
(34) Ozawa, H.; Ide, N.; Fujigaya, T.; Niidome, Y.; Nakashima, N. One-pot separation of highly enriched (6,5)-single-walled carbon nanotubes using a fluorene-based copolymer. *Chem. Lett.* **2011**, *40*, 239−241.
(35) Mistry, K. S.; Larsen, B. A.; Blackburn, J. L. High-yield dispersions of large-diameter semiconducting single-walled carbon nanotubes with tunable narrow chirality distributions. *ACS Nano* **2013**, *7*, 2231−2239.
(36) Gomulya, W.; Gao, J.; Loi, M.A. Conjugated polymer-wrapped carbon nanotubes: physical properties and device applications, *Eur. Phys. J. B* **2013**, *86* DOI: 10.1140/epjb/e2013-40707-9.
(37) Nish, A.; Hwang, J.-Y.; Doig, J.; Nicholas, R. J. Highly selective dispersion of single-walled carbon nanotubes using aromatic polymers. *Nat. Nanotechnol.* **2007**, *2*, 640−646.
(38) Ozawa, H.; Fujigaya, T.; Niidome, Y.; Hotta, N.; Fujiki, M.; Nakashima, N. Rational concept to recognize/extract single-walled carbon nanotubes with a specific chirality. *J. Am. Chem. Soc.* **2011**, *133*, 2651−2657.
(39) Samanta, S. K.; Fritsch, M.; Scherf, U.; Gomulya, W.; Bisri, S. Z.; Loi, M. A. Conjugated polymer-assisted dispersion of single-wall carbon nanotubes: the power of polymer wrapping. *Acc. Chem. Res.* **2014**, *47*, 2446−2456.
(40) Berton, N.; Lemasson, F.; Poschlad, A.; Meded, V.; Tristram, F.; Wenzel, W.; Hennrich, F.; Kappes, M. M.; Mayor, M. Selective dispersion of large-diameter semiconducting single-walled carbon

DOI: 10.1021/acs.jpcc.9b04869
J. Phys. Chem. C 2019, 123, 24807−24817

nanotubes with pyridine-containing copolymers. *Small* **2014**, *10*, 360−367.
(41) Minoia, A.; Chen, L.; Beljonne, D.; Lazzaroni, R. Molecular modeling study of the structure and stability of polymer/carbon nanotube interfaces. *Polymer* **2012**, *53*, 5480−5490.
(42) Haghighatpanah, S.; Bolton, K. Molecular-level computational studies of single wall carbon nanotube−polyethylene composites. *Comput. Mater. Sci.* **2013**, *69*, 443−454.
(43) Bohlén, M.; Bolton, K. Molecular dynamics studies of the influence of single wall carbon nanotubes on the mechanical properties of Poly(vinylidene fluoride). *Comput. Mater. Sci.* **2013**, *68*, 73−80.
(44) Zheng, Q.; Xue, Q.; Yan, K.; Hao, L.; Li, Q.; Gao, X. Investigation of molecular interactions between swnt and polyethylene/polypropylene/polystyrene/polyaniline molecules. *J. Phys. Chem. C* **2007**, *111*, 4628−4635.
(45) Gerstel, P.; Klumpp, S.; Hennrich, F.; Poschlad, A.; Meded, V.; Blasco, E.; Wenzel, W.; Kappes, M. M.; Barner-Kowollik, C. Highly selective dispersion of single-walled carbon nanotubes via polymer wrapping: a combinatorial study via modular conjugation. *ACS Macro Lett.* **2014**, *3*, 10−15.
(46) Gurevitch, I.; Srebnik, S. Monte Carlo simulation of polymer wrapping of nanotubes. *Chem. Phys. Lett.* **2007**, *444*, 96−100.
(47) Yang, H.; Bezugly, V.; Kunstmann, J.; Filoramo, A.; Cuniberti, G. Diameter-selective dispersion of carbon nanotubes via polymers: a competition between adsorption and bundling. *ACS Nano* **2015**, *9*, 9012−9019.
(48) Hunter, C. A.; Sanders, J. K. M. The nature of pi-pi interactions. *J. Am. Chem. Soc.* **1990**, *112*, 5525−5534.
(49) Gao, J.; Kwak, M.; Wildeman, J.; Herrmann, A.; Loi, M. A. Effectiveness of sorting single-walled carbon nanotubes by diameter using polyfluorene derivatives. *Carbon* **2011**, *49*, 333−338.
(50) Dai, H.; Rinzler, A. G.; Nikolaev, P.; Thess, A.; Colbert, D. T.; Smalley, R. E. Single-wall nanotubes produced by metal-catalyzed disproportionation of carbon monoxide. *Chem. Phys. Lett.* **1996**, *260*, 471−475.
(51) Kitiyanan, B.; Alvarez, W. E.; Harwell, J. H.; Resasco, D. E. Controlled production of single-wall carbon nanotubes by catalytic decomposition of CO on bimetallic Co−Mo catalysts. *Chem. Phys. Lett.* **2000**, *317*, 497−503.
(52) Frisch, M. J.; Trucks, G. W.; Schlegel, H. B.; Scuseria, G. E.; Robb, M. A.; Cheeseman, J. R.; Scalmani, G.; Barone, V.; Mennucci, B.; Petersson, G.A., et al., *Gaussian 09*; Gaussian, Inc.: Wallingford, CT, 2009.
(53) Lee, C.; Yang, W.; Parr, R. G. Development of the Colle-Salvetti correlation-energy formula into a functional of the electron density. *Phys. Rev. B: Condens. Matter Mater. Phys.* **1988**, *37*, 785−789.
(54) Becke, A. D. Density-functional thermochemistry. III. The role of exact exchange. *J. Chem. Phys.* **1993**, *98*, 5648−5652.
(55) Vosko, S. H.; Wilk, L.; Nusair, M. Accurate spin-dependent electron liquid correlation energies for local spin density calculations: a critical analysis. *Can. J. Phys.* **1980**, *58*, 1200−1211.
(56) Hariharan, P. C.; Pople, J. A. The influence of polarization functions on molecular orbital hydrogenation energies. *Theor. Chim. Acta.* **1973**, *28*, 213−222.
(57) Ditchfield, R.; Hehre, W. J.; Pople, J. A. Self-Consistent Molecular-Orbital Methods. IX. An extended gaussian-type basis for molecular-orbital studies of organic molecules. *J. Chem. Phys.* **1971**, *54*, 724−728.
(58) Collins, J. B.; Schleyer, P. v. R.; Binkley, J. S.; Pople, J. A. Self-consistent molecular orbital methods. XVII. Geometries and binding energies of second-row molecules. A comparison of three basis sets. *J. Chem. Phys.* **1976**, *64*, 5142−5151.
(59) Kilina, S.; Kilin, D.; Tretiak, S. Light-driven and phonon-assisted dynamics in organic and semiconductor nanostructures. *Chem. Rev.* **2015**, *115*, 5929−5978.
(60) Kilina, S.; Batista, E. R.; Yang, P.; Tretiak, S.; Saxena, A.; Martin, R. L.; Smith, D. L. Electronic structure of self-assembled amorphous polyfluorenes. *ACS Nano* **2008**, *2*, 1381−1388.
(61) Kilina, S.; Dandu, N.; Batista, E. R.; Saxena, A.; Martin, R. L.; Smith, D. L.; Tretiak, S. Effect of packing on formation of deep carrier traps in amorphous conjugated polymers. *J. Phys. Chem. Lett.* **2013**, *4*, 1453−1459.
(62) Allinger, N. L.; Yuh, Y. H.; Lii, J. H. Molecular mechanics. The MM3 force field for hydrocarbons. 1. *J. Am. Chem. Soc.* **1989**, *111*, 8551−8566.
(63) Lii, J. H.; Allinger, N. L. Molecular mechanics. The MM3 force field for hydrocarbons. 2. Vibrational frequencies and thermodynamics. *J. Am. Chem. Soc.* **1989**, *111*, 8566−8575.
(64) Lii, J. H.; Allinger, N. L. Molecular mechanics. The MM3 force field for hydrocarbons. 3. The van der Waals' potentials and crystal data for aliphatic and aromatic hydrocarbons. *J. Am. Chem. Soc.* **1989**, *111*, 8576−8582.
(65) Allinger, M. L.; Li, F.; Yan, L. Molecular Mechanics. The MM3 force field for alkenes. *J. Comput. Chem.* **1990**, *11*, 848−867.
(66) Fricker, J. Jack Tinker. *BMJ* **2010**, *340*, c2920.
(67) Frey, J. T.; Doren, D. J. *TubeGen 3.4*; University of Delaware: Neward, DE, 2011.
(68) Kilina, S.; Yarotski, D. A.; Talin, A. A.; Tretiak, S.; Taylor, A. J.; Balatsky, A. V. Unveiling stability criteria of DNA-carbon nanotubes constructs by scanning tunneling microscopy and computational modeling, *J. Drug Delivery* **2011**, *2011*, 1.
(69) Shea, M. J.; Mehlenbacher, R. D.; Zanni, M. T.; Arnold, M. S. Experimental measurement of the binding configuration and coverage of chirality-sorting polyfluorenes on carbon nanotubes. *J. Phys. Chem. Lett.* **2014**, *5*, 3742−3749.
(70) Bachilo, S. M.; Balzano, L.; Herrera, J. E.; Pompeo, F.; Resasco, D. E.; Weisman, R. B. Narrow (n, m)-distribution of single-walled carbon nanotubes grown using a solid supported catalyst. *J. Am. Chem. Soc.* **2003**, *125*, 11186−11187.

DOI: 10.1021/acs.jpcc.9b04869
J. Phys. Chem. C 2019, 123, 24807−24817